J Physiol 589.8 (2011) pp 1927–1941

The Journal of Physiology

Loss of olfactory cell adhesion molecule reduces the synchrony of mitral cell activity in olfactory glomeruli

Maria Borisovska, Matthew J. McGinley, AeSoon Bensen and Gary L. Westbrook

Vollum Institute, Oregon Health and Science University, Portland, OR 97239, USA

Non-technical summary In olfactory bulb glomeruli, incoming sensory input from the nose (axodendritic synapses) is segregated from local intraglomerular interactions (dendrodendritic synapses). We examined the synchrony of neural activity within glomeruli using knockout mice in which loss of olfactory cell adhesion molecule disrupts clustering of synaptic compartments. Using paired whole-cell recording of mitral cells within a single glomerulus in brain slices, synchrony of fast and slow neural activity was reduced. However, incoming afferent activity and dendrodendritic inhibition were unaffected. We suggest that compartmentalization of synapses in the glomerulus is important for processing of olfactory sensory information.

Abstract Odours generate activity in olfactory receptor neurons, whose axons contact the dendritic tufts of mitral cells within olfactory bulb glomeruli. These axodendritic synapses are anatomically separated from dendrodendritic synapses within each glomerulus. Mitral cells within a glomerulus show highly synchronized activity as assessed with whole-cell recording from pairs of mitral cells. We examined glomerular activity in mice lacking the olfactory cell adhesion molecule (OCAM). Glomeruli in mice lacking OCAM show a redistribution of synaptic subcompartments, but the total area occupied by axonal inputs was similar to wild-type mice. Stimulation of olfactory nerve bundles showed that excitatory synaptic input to mitral cells as well as dendrodendritic inhibition was unaffected in the knockout. However, correlated spiking in mitral cells was significantly reduced, as was electrical coupling between apical dendrites. To analyse slow network dynamics we induced slow oscillations with a glutamate uptake blocker. Evoked and spontaneous slow oscillations in mitral cells and external tufted cells were broader and had multiple peaks in OCAM knockout mice, indicating that synchrony of slow glomerular activity was also reduced. To assess the degree of shared activity between mitral cells under physiological conditions, we analysed spontaneous sub-threshold voltage oscillations using coherence analysis. Coherent activity was markedly reduced in cells from OCAM knockout mice across a broad range of frequencies consistent with a decrease in tightly time-locked activity. We suggest that synchronous activity within each glomerulus is dependent on segregation of synaptic subcompartments.

(Resubmitted 26 January 2011; accepted after revision 17 February 2011; first published online 21 February 2011)
Corresponding author M. Borisovska: Vollum Institute, Oregon Health and Science University, Portland, OR 97239, USA. Email: maria.borisovska@gmail.com

Abbreviations EPSC, excitatory postsynaptic current; EPSP, excitatory postsynaptic potential; IPSC, inhibitory postsynaptic current; NCAM, neuronal cell adhesion molecule; OCAM, olfactory cell adhesion molecule; OMP, olfactory marker protein.

DOI: 10.1113/jphysiol.2011.206276

Introduction

Olfactory receptor neurons that express the same odorant receptor project into specific glomeruli where they synapse with apical dendrites of the mitral cells, the principal neurons of the olfactory bulb (Buck & Axel, 1991; Mombaerts *et al.* 1996). The glomerulus is generally viewed as a functional unit capable of receiving, processing and sending out odour-specific information (Chen & Shepherd, 2005; Fantana *et al.* 2008). Mitral cells receiving input from the same glomerulus exhibit a specific pattern of membrane voltage oscillations and synchronized activity (Schoppa & Urban, 2003; Kay *et al.* 2009). Such rhythmic activity has been hypothesized to underlie the transformation of the spatial map of odour-activated glomeruli into a time–frequency code (Laurent, 2002). The voltage oscillations reflect local glomerular microcircuit interactions between inputs from olfactory receptor neurons and the dendrites of mitral cells and juxtaglomerular cells. Morphological studies have revealed a complex anatomical organization of glomeruli with distinct axonal and dendritic subcompartments, consisting primarily of axodendritic and dendrodendritic synapses, respectively (Kosaka *et al.* 1998; Kasowski *et al.* 1999; Kim & Greer, 2000). Astrocytic processes separate excitatory axodendritic synapses made by axons of olfactory receptor neurons and dendrites of mitral and juxtaglomerular cells from dendrodendritic synapses between mitral and juxtaglomerular cells (Pinching & Powell, 1971; Chao *et al.* 1997; de Saint Jan & Westbrook, 2005).

Olfactory cell adhesion molecule (OCAM) is a member of the immunoglobulin superfamily that is expressed in developing and adult olfactory receptor neurons and in mitral cells (Yoshihara *et al.* 1997; Treloar *et al.* 2003). Based on its spatiotemporal expression pattern, OCAM was initially considered a candidate for targeting of olfactory receptor neurons expressing the same odour receptor to specific glomeruli. Although analysis of the OCAM knockout mouse revealed no change in targeting or distribution of axons entering the olfactory bulb, organization of axodendritic and dendrodendritic synapses within glomeruli was disrupted, indicating a role for OCAM in compartmentalization of synapses within the glomerular layer (Walz *et al.* 2006). Here, we examined whether loss of OCAM affected mitral cell activity within glomeruli. For physiological studies, acute slices of olfactory bulb were prepared from P22–30 mice. Paired whole-cell recordings in mitral cells were used to probe neuronal activity patterns within glomeruli, and confocal imaging of fixed tissue was used to quantify glomerular subcompartments. The loss of OCAM did not alter EPSCs evoked by focal stimulation of olfactory nerve bundles. However, intraglomerular synchrony of both fast and slow activity was reduced, as measured by paired mitral cell recordings.

Methods

Mice

The OCAM knockouts were originally generated in a mixed 129/C57Bl/6 background, but then crossed for more than nine generations with C57Bl/6 mice to assure >99% C57Bl/6 genetic background (Green, 1966). We used OCAM knockout mice as well as OCAM knockout crossed with Thy-1 transgenic mice (C57Bl/6) that express YFP (line YFP-G) in a subset of mitral/tufted cells (Feng *et al.* 2000; Walz *et al.* 2006). The expression of YFP did not alter mitral cells' responses, and so data from both lines were pooled and referred to as knockout. C57BL/6 and Thy-1 transgenic mice were used as wild-type controls. P22–30 mice were used for electrophysiological and histological experiments. The animal protocols were approved by the Institutional Animal Care and Use Committee and followed the National Institutes of Health guidelines for the ethical treatment of animals.

Immunohistochemistry and its quantification

Mice were deeply anaesthetized using avertin (250 mg kg^{-1}) injected intraperitoneally and were intracardially perfused with ice-cold PBS followed by 4% (w/v) paraformaldehyde (PFA) in PBS. Brains were post-fixed in 4% PFA overnight and embedded in a 2.5% agarose solution. Horizontal sections (100 μm) were cut with a vibrating-blade microtome (Leica VT1000), and incubated with goat anti-OMP (1:1000, 544-10002-WAKO). Primary antibodies were detected with secondary antibodies conjugated with Cy5 (Molecular Probes, A-11057). Images were obtained using a LSM 710 confocal microscope (Zeiss, Germany) and 40× C-Apo (1.2 NA) objective. To visualize OMP-labelled axons, we used a DPSS 561 nm laser, and images were acquired from horizontal sections of the glomerular cell layer at 8-bit resolution. To quantify clustering of axonal and dendritic subcompartments, we placed a grid (3.5 μm × 3.5 μm each square) on each image of a glomerulus using Metamorph software. Glomeruli contained 411 ± 46 and 488 ± 63 squares for wild-type and knockout, respectively. For each square, we calculated the fraction that was OMP positive (axodendritic subcompartment) as the area above a threshold level of 40 (0–255 scale). We analysed glomeruli in both the ventrolateral olfactory bulb where OCAM is expressed in axons, and in the dorsomedial olfactory bulb where OCAM is expressed in mitral cell dendrites (Walz *et al.*

2006; data not shown). Both areas showed altered compartmentalization and thus were considered together for this analysis.

Electrophysiology

Horizontal slices of the main olfactory bulb (300 μm) were cut using a Leica VT 1200 S vibrating-blade microtome. The ice-cold oxygenated cutting solution contained: 83 mM NaCl, 26.2 mM $NaHO_3$, 2.5 mM KCl, 1 mM NaH_2PO_4, 3.3 mM $MgCl_2$, 0.5 mM $CaCl_2$, 22 mM glucose, and 72 mM sucrose (pH 7.3). Slices were incubated for 30–40 min at 33–34°C, and then kept at room temperature for at least 30 min prior to experiment in recording solution of composition: 125 mM NaCl, 25 mM $NaHO_3$, 3 mM KCl, 1.25 mM NaH_2PO_4, 1 mM $MgCl_2$ and 2 mM $CaCl_2$. Whole-cell current clamp recordings were done at room temperature to minimize neuronal network self-excitation. Cells were patched under visual control using DIC optics and an ORCA II camera (Hamamatsu). Patch pipettes (4–6 MΩ) contained: 135 mM potassium gluconate, 1 mM EGTA, 2 mM MgATP, 0.5 mM NaGTP, 12 mM Hepes and 10 μM Alexa 555 (pH 7.3). For probing dendrodendritic inhibition potassium glutamate was replaced with KCl. Recordings were made with a Multiclamp 700B amplifier (Molecular Devices, Sunnyvale, CA, USA). The analog signals were filtered at 10 kHz with the built-in Bessel filter and digitized at 5–10 kHz. Data were acquired with Axograph X. For theta pipette stimulation of olfactory axon bundles innervating single glomeruli, we used borosilicate theta pipettes (tip opening 1–2 μm, Sutter Instrument Co., Novato, CA, USA) that were filled with recording solution. To allow direct visualization of nerve bundles entering specific glomeruli, these recordings were done in the medial portion of the slice. To record dendrodendritic inhibition, the olfactory nerve layer was stimulated with bipolar stainless steel electrodes (tip separation of 200 μm; FHC Inc., Bowdoin, ME, USA). Stimulus pulses (100 μs, 20 V for bipolar electrode; 100 μs, 50–100 V for theta pipette) were applied using a stimulus isolation unit (DS2A; Digitimer Ltd, Welwyn Garden City, UK). To stimulate slow membrane oscillations, 40 μM DL-threo-β-benzyloxyaspartic acid (TBOA) was bath applied for 5 min prior to recording to obtain regular oscillations, and one recording was performed per slice. We used paired recordings of mitral cells to probe spike synchrony and electrical coupling (see below) within a glomerulus. Most mitral cell pairs were recorded in the medial half of the olfactory bulb because it was easier to identify pairs of mitral cells that projected to the same glomerulus. External tufted cells were identified by their location, morphology, large soma and relatively low input resistance (Hayar *et al.* 2004*a*). Periglomerular cells remained quiet even after long TBOA applications and, thus, were unlikely to be misidentified as external tufted cells. Steady hyperpolarizing current injections were often used to prevent random spiking in mitral cells and external tufted cells. Alexa Fluor 555 (Molecular Devices) was routinely added to the internal solution to visualize cellular morphology. Drugs were purchased from Tocris (Ellisville, MO, USA) or Ascent Scientific (Bristol, UK) as follows: 6-nitro-7-sulfamoylbenzo[f]quinoxaline-2,3-dione (NBQX), DL-2-amino-5-phosphonovaleric acid (AP5), 7-(hydroxyimino)cyclopropa[b]chromen-1a-carboxylate ethyl ester (CPCCOEt), DL-*threo*-β-benzyloxyaspartic acid (TBOA), 6-imino-3-(4-methoxyphenyl)-1(6*H*)-pyridazinebutanoic acid hydrobromide (SR95531).

Analysis

Electrophysiological data were exported from Axograph into IGOR Pro (WaveMetrics, Inc., Lake Oswego, OR, USA) using the Neuromatic routine (Jason Rothman, http://www.neuromatic.thinkrandom.com). Custom IGOR Pro routines were used for all analyses except coherence analysis, which was performed in Matlab. For dendro-dendritic inhibition, the amplitude was calculated for the interval between 50 and 100 ms after stimulation. Charge was calculated for the 3.5 s following stimulation. For theta pipette evoked responses, 10 subsequent sweeps were averaged to reduce the noise. The rising phase of the fast component was fitted with monoexponential. The synaptic delay was determined as a time lag between the stimulation and the time point when amplitude of the response exceeded RMS noise 5-fold. The amplitude of the slow component was determined as the average between 375 and 425 ms after the stimulation. To assess spike synchrony between pairs of mitral cells, depolarizing current injections (2–4 s) into both mitral cells were adjusted to evoke spiking at 10–20 Hz (13.4 ± 3.8 Hz and 13.4 ± 3.1 Hz for wild-type and knockout respectively). We then chose the cell with fewer spikes, and determined a time lag between each spike for this cell and the closest spike in the paired cell. Time lags of ±200 ms were plotted for bar graphs. Bar graphs for each individual mitral cell pair (5 ms bins) were averaged to compare wild-type and knockout. A synchrony coefficient was defined as the ratio between the frequency of time lags of $|dt| < 10$ ms and time lags $30\text{ ms} < |dt| < 50$ ms (see Fig. 2, areas highlighted in grey). Excess kurtosis was calculated using a standard formula:

$$\kappa = \frac{(n+1)n}{(n-1)(n-2)(n-3)} \times \frac{\sum_{i=1}^{n}(x_i-\bar{x})^4}{(\sigma^2)^2} - 3 \times \frac{(n-1)^2}{(n-1)(n-3)},$$

where σ^2 is the variance, $\bar{x}$ is a sample mean, n is a total number of values, x_i is the ith value.

To measure electrical coupling between mitral cells, a hyperpolarizing current step (250 ms, 200–250 pA) was applied to one of the cells in the pair and voltage responses of both cells was recorded. Bidirectional coupling coefficients were determined per pair and averaged. Twenty sweeps were averaged per cell to reduce noise. Membrane voltages were measured over a time period of 40 ms, 10 ms before the stimulation and 250–300 ms after the start of hyperpolarization. The coupling coefficient was determined as the ratio of the hyperpolarization in the follower cell over that in the stimulated cell. For slow oscillations, the following parameters were determined for each voltage envelope: peak amplitude, area, half-width and 20–70% rise time. To analyse oscillations that appeared to have more than one peak, we used the following criteria. If the minimum point between two peaks was greater than 20% of the lower peak and less than 80% of the main peak, the oscillation was considered to have two peaks. For envelopes with more than two peaks, only the two major ones were analysed. To analyse coherence between spontaneous subthreshold activities in pairs of mitral cells, 2–5 s epochs (20–30 per pair) were selected for each pair of mitral cells. The epoch length for each pair was determined based on the frequency and duration of spontaneous oscillations. Coherence, power spectrum and phase uncertainty were calculated using a multitaper method with custom written code (M. J. McGinley & G. L. Westbrook, unpublished; MATLAB 7.10, The Mathworks, Inc., Natick, MA, USA; Percival & Walden, 1993; Huybers, 2004). Phase uncertainty was defined as the width of a 95% bootstrap confidence interval (Zoubir, 2009), of the coherence phase at each frequency, calculated across epochs for each pair (M. J. McGinley & G. L. Westbrook, unpublished). Depending on epoch length, between 6 and 12 tapers were used to target a consistent resolution bandwidth, f_0, of 2.6–3.2 Hz. $f_0 = (T + 1)/(N\mathrm{d}t)$, where T is the number of tapers, N is the number of data points per sweep, and $\mathrm{d}t$ is the time between adjacent data points (Percival & Walden, 1993). Coherence is constrained to a range from 0 to 1, but the analysis used gives a baseline coherence value of approximately 0.2 across the frequency range even for uncorrelated signals, and thus the effective range is 0.2–1.0 (M. J. McGinley, unpublished). Unmatched epochs for each pair were used to calculate the baseline coherence.

Statistics

Student's t test was used where appropriate. Significance was displayed at $^{*}P \leq 0.05$; $^{**}P \leq 0.01$ and $^{***}P \leq 0.001$. Data were expressed as the mean ± SEM. Coherence and phase estimates were compared using Kruskal–Wallis ANOVA followed by the Mann–Whitney U test with a Newman–Keuls correction. To account for resolution bandwidth (see above) coherence or phase-uncertainty estimates were considered to be significantly different only when more than four consecutive frequencies showed significantly different coherence.

Results

Loss of OCAM leads to desegregation of olfactory receptor neuron axons

Axodendritic and dendrodendritic synapses within glomeruli are more heterogeneously distributed as seen in electron micrographs of OCAM knockout animals (Walz *et al.* 2006). To verify the impact of OCAM on the segregation of synaptic subcompartments across glomeruli, we labelled afferent axons entering olfactory bulb glomeruli with olfactory marker protein (OMP, Fig. 1*A*, Baker *et al.* 1989). To quantify the clustering, we superimposed a grid on confocal images of glomeruli across all quadrants of the olfactory bulb, and determined the fraction of OMP-positive labelling within each grid square (see methods). We analysed glomeruli in the ventrolateral olfactory bulb, where OCAM is expressed in axons, and in the dorsomedial olfactory bulb, where OCAM is expressed in mitral cell dendrites (Walz *et al.* 2006; see methods). As shown in Fig. 1*B*, wild-type animals showed highly segregated labelling with many of the grid squares either unlabelled with OMP (dendrodendritic) or nearly completely labelled with OMP (axodendritic). However, there was a redistribution of OMP-labelled areas in the OCAM knockout mice, as seen by the increased number of squares containing both OMP-positive and -negative areas (Fig. 1*B* and inset). The total glomerular area that was labelled with OMP was similar in wild-type (66.4 ± 1.7%) and knockout (62.3 ± 1.9%), suggesting that it is not the number of olfactory receptor axons, but rather their spatial distribution that is disrupted in the absence of OCAM.

Afferent excitation and dendrodendritic inhibition are preserved in the OCAM knockout

To assess the synaptic input of olfactory receptor neurons to a glomerulus, we used focal stimulation with theta pipette (1–2 μm tip) to activate bundles of olfactory sensory axons as they entered a glomerulus and contact mitral cell dendrites (Fig. 2*A*). Stimulation at 20 Hz revealed short latency excitatory postsynaptic potentials in mitral cells in both wild-type and OCAM knockout (Fig. 2*B*). There was no difference in the delay or rise time (tau) of the response between wild-type and OCAM

knockouts (Fig. 2*C*). The EPSP could not be evoked when the stimulation pipette was moved 20–30 μm away from the visually identified bundle, consistent with glomerular-specific activation (not shown). The lack of jitter in the synaptic latency confirmed that these EPSPs represent the fast monosynaptic afferent input. As previously described (de Saint Jan & Westbrook, 2007), the fast initial peak of the EPSP was followed by a slow component that lasted several seconds (WT: 2.6 ± 0.4 s; OCAM KO: 2.6 ± 0.4 s; Fig. 2*D*). CPCCOEt and AP5 that block mGluR1 and NMDA receptors eliminated the slow component. The addition of NBQX to block AMPA receptors blocked the remaining fast component. The slow component in the OCAM knockout showed the same pharmacological profile (Fig. 2*D* and *E*), suggesting that the afferent input to mitral cell dendrites is intact in OCAM knockout mice.

Activation of excitatory synapses in axodendritic subcompartments subsequently triggers dendrodendritic inhibition, one of the most characteristic features of the olfactory bulb network. At dendrodendritic synapses, glutamate released from mitral cell dendrites activates GABAergic interneurons, leading to GABA release back onto mitral cell dendrites. To test whether loss of OCAM affected dendrodendritic inhibition, we stimulated the olfactory nerve layer with a bipolar electrode (200 μm tip spacing) and recorded from mitral cells. Because of the reciprocal expression of OCAM, we tested both dorsomedial and ventrolateral glomeruli. Electrical stimulation in both wild-type and OCAM knockout mitral cells evoked fast inward excitatory current followed by a slow polysynaptic IPSC (Fig. 3*A*), which was reduced by the $GABA_A$ receptor antagonist SR 95531. The total inhibitory current, as measured by integrating the charge over the first 3.5 s following stimulation, was unchanged in the OCAM knockout compared to wild-type (Fig. 3*A* and *B*). SR 95531 appeared to be slightly less effective in the OCAM knockout, but this did not reach statistical significance (Fig. 3*C*). The similarities between the wild-type and knockout mitral cell afferent excitation and dendrodendritic inhibition suggests that the general pattern of excitation and inhibition is preserved in the OCAM knockout. There were also no apparent differences in the morphological organization of the glomerular layer or in glomerular size (see online Supplemental Material, Supplementary Fig. 1).

Reduced spike synchrony and electrical coupling in the OCAM knockout

Mitral cells within a glomerulus show highly correlated activity that is dependent on interactions between axodendritic and dendrodendritic synapses. Thus, we asked whether intraglomerular neural activity was altered

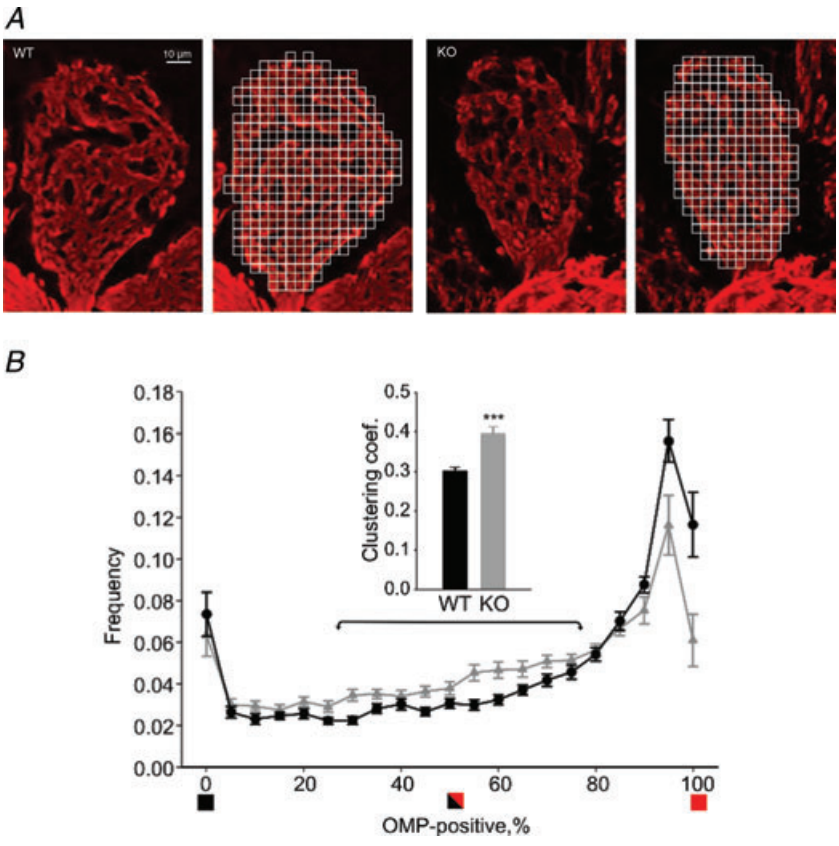

Figure 1. OCAM disrupts compartmentalization of axonal and dendritic profiles within olfactory bulb glomeruli
A, olfactory bulb glomeruli from wild-type (left) and OCAM knockout (right) were immunostained with an anti-olfactory marker protein (OMP) antibody (red). The labelled areas represent axodendritic subcompartments whereas the unlabelled areas are dendrodendritic subcompartments. We superimposed a grid of 3.5 μm squares (to the right) and calculated the fraction of OPM-positivity within each square. *B*, the bar graph plots the number of grid squares as a function of the percentage of OMP-labelled area within the square. Wild-type glomeruli showed a large number of grid squares that were completely OMP-positive squares (black circles), whereas the OCAM knockout had squares with a mix of labelled and unlabelled areas (grey triangles). The clustering coefficient as computed for squares in the 25–75% range (arrows) was higher for the knockout. ***$P < 0.001$. The bar graph shows data from 20 wild-type glomeruli and 19 OCAM knockout glomeruli with 3 animals in each group.

in OCAM knockout mice. Mitral cells send their apical dendrite to a single glomerulus, and mitral cells that receive input from the same glomerulus exhibit synchronous spiking (Schoppa & Westbrook, 2001). To visualize mitral cells that project to the same glomerulus, we crossed wild-type and OCAM knockout mice with Thy1-YFP mice (line YFP-G, Feng *et al.* 2000) in which YFP is expressed in a subpopulation of mitral/tufted cells (Fig. 4*A*). Simultaneous whole-cell current clamp recordings were performed on pairs of mitral cells. Long

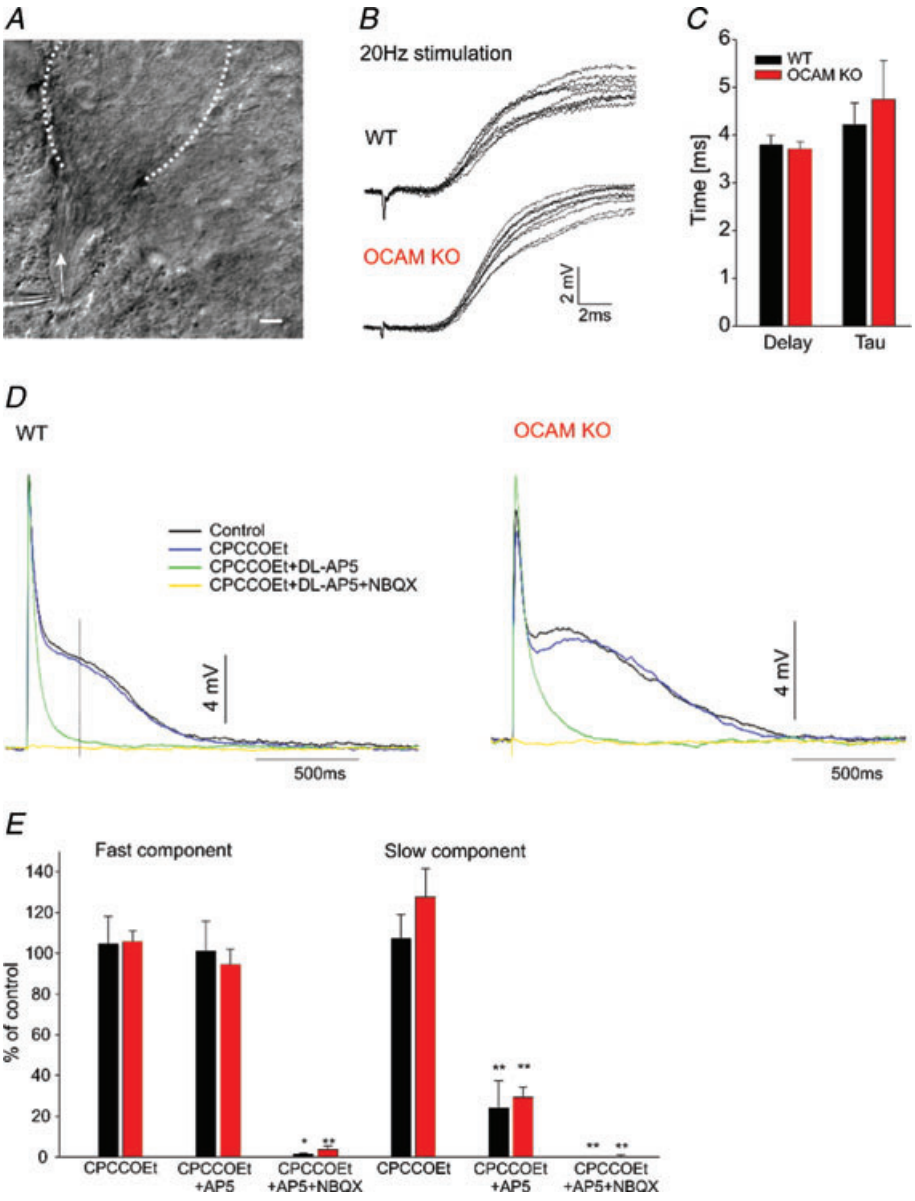

Figure 2. Olfactory nerve evoked EPSPs are unchanged in the OCAM knockouts
A, light microscopy image of theta pipette stimulating olfactory axon bundle (arrow) entering a glomerulus (dashed lines). Scale: 10 μm. *B*, exemplary recordings of WT (upper panel) and OCAM KO (lower panel) monosynaptic EPSPs stimulated at 20 Hz at high time resolution. Note the stimulation artifact. *C*, kinetics analysis of the fast component (shown in *B*) revealed similar time constant (tau) of monoexponential fitting for WT (black, $n = 9$) and OCAM knockout (red, $n = 7$). The onset of the monosynaptic EPSP occurred with the same delay. *D*, exemplary full scale EPSP showed a fast monosynaptic and a slow component in both WT (left panel) and OCAM KO (right panel) mitral cells. The mGluR1 antagonist CPCCOEt (100 μM, blue) has little effect on the EPSP. The NMDA antagonist AP5 (150 μM, green) abolished slow component but did not affect the fast component. Subsequent addition of the AMPA receptor blocker NBQX (20 μM, yellow) completely blocked the EPSP. *E*, quantification of responses shown in *D*. The amplitude of the fast component was not affected by CPCCOEt (WT: $n = 7$, KO: $n = 9$) or AP5 (WT: $n = 6$, KO: $n = 5$). The amplitude of the slow component was measured 250 ms after stimulation. $^{*}P < 0.05$, $^{**}P < 0.01$, paired *t* test.

depolarizing current pulses evoked low frequency firing (*ca* 13 Hz, see methods) in each cell (Fig. 4*B*). In wild-type mice, plots of the lags between spikes in pairs of mitral cells showed a peak at 0 ms, consistent with correlated spiking (Fig. 4*C*, black trace). However, in OCAM knockout mice, the peak at 0 ms was much smaller and the spread of the lags was much broader (Fig. 4*C*, red trace). We quantified these differences as the ratio of the lags at ±10 ms compared to lags in the −30 to −50 ms interval (Fig. 4*C*, grey bars, synchrony coefficient) and as excess kurtosis (Fig. 4*D* and *E*). Both parameters were reduced for the knockout. Thus in OCAM knockout mice, the synchrony of mitral cell spiking within a glomerulus was reduced.

In mice lacking connexin 36, correlated spiking is completely abolished, indicating that gap junctions between mitral cell dendrites are required for intra-glomerular spike synchrony (Christie *et al.* 2005). Thus, we measured electrical coupling between mitral cells in OCAM knockout mice. In wild-type cell pairs, hyperpolarizing current injections in one cell caused a hyperpolarization in the follower cell, consistent with electrical coupling (Fig. 4*F*, left panel). The coupling coefficient in OCAM knockouts was 0.037 ± 0.005 compared to 0.059 ± 0.007 in the wild-type (Fig. 4*G*). The input resistance of mitral cells was unaffected by loss of OCAM (Fig. 4*H*), indicating that the reduction in coupling coefficient was not an indirect effect of changes in membrane conductance (Maher *et al.* 2009). Thus loss of OCAM reduces correlated spiking between mitral cells in the glomerulus as well as the electrical coupling between mitral cell dendrites.

Slow oscillations in mitral and external tufted cells

Glomeruli also show rhythmic activity on a slow time scale. For example, olfactory nerve stimulation or an increase in extracellular glutamate cause mitral cells to oscillate at 0.5–2 Hz (Carlson *et al.* 2000; Puopolo & Belluzzi, 2001; Schoppa & Westbrook, 2001). Glutamate spillover plays an important role in generating such slow activity (Isaacson, 1999; Christie & Westbrook, 2006). To stimulate slow oscillations in mitral cells, we bath-applied the glutamate reuptake blocker TBOA (40 μM). TBOA elicited robust oscillations in slices in mitral cells from both wild-type and knockout mice, but multi-peaked oscillations were much more common in the knockout (Fig. 5*A*). This fraction of multi-peaked events was increased in both dorso-medial and ventrolateral glomeruli in the knockout (DM: 0.56 ± 0.09 KO, 0.16 ± 0.06 WT, $n = 5$; VL: 0.44 ± 0.02 KO, 0.13 ± 0.04 WT, $n = 4$). We analysed the shape of the slow oscillations using the parameters shown in Fig. 5*B*. Although multi-peaked events were more common in the knockout, measures of the shape of these oscillations were similar to the occasional multi-peaked events in wild-type (Fig. 5*C*). Multi-peaked events had the same amplitude, but an increase in half-width and area compared to

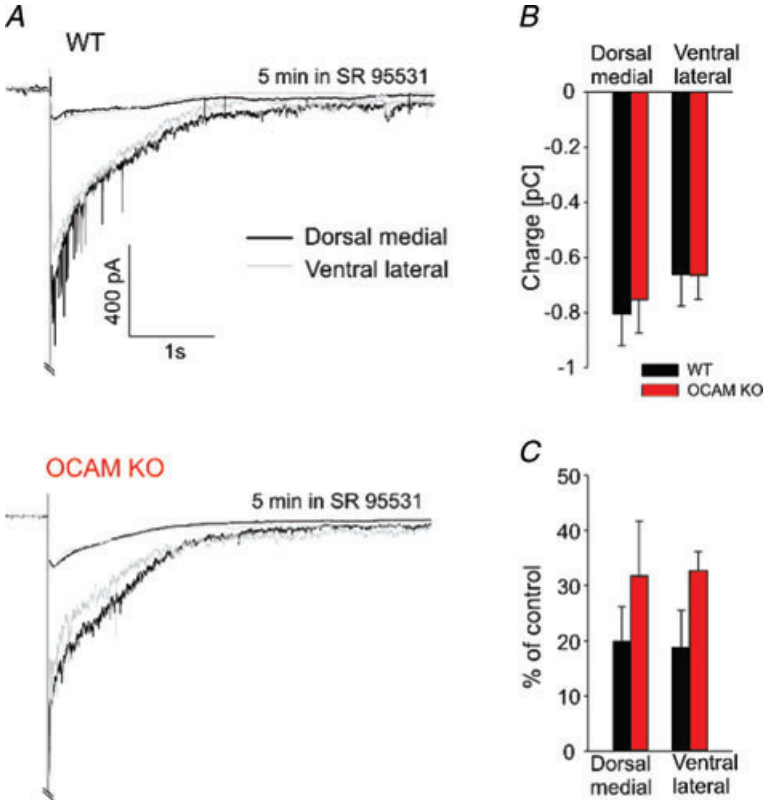

Figure 3
Dendrodendritic inhibition is preserved in the OCAM knockout glomeruli. A Bipolar stimulation of the glomerular layer elicited a long-lasting inward current in mitral cells in wild-type (top) and OCAM knockouts (bottom) in both dorsomedial (black, WT: $n = 8$, KO: $n = 10$) and ventrolateral (grey, WT: $n = 5$, KO: $n = 9$) regions of the bulb. The responses was strongly diminished by the $GABA_A$ receptor antagonist SR 95531 (upper trace), indicating preserved $GABA_A$ receptor mediated inhibition from granular and periglomerular cells in the OCAM knockout. Traces represent averages of all recorded cells. *B*, the overall charge of dendrodendritic inhibition, measured at 3.5 s after the stimulation, was unchanged in OCAM knockouts. *C*, SR 95531 reduced dendrodendritic inhibition in mitral cells (dorsomedial: WT: $n = 8$, KO: $n = 6$; ventrolateral: WT: $n = 5$, KO: $n = 4$).

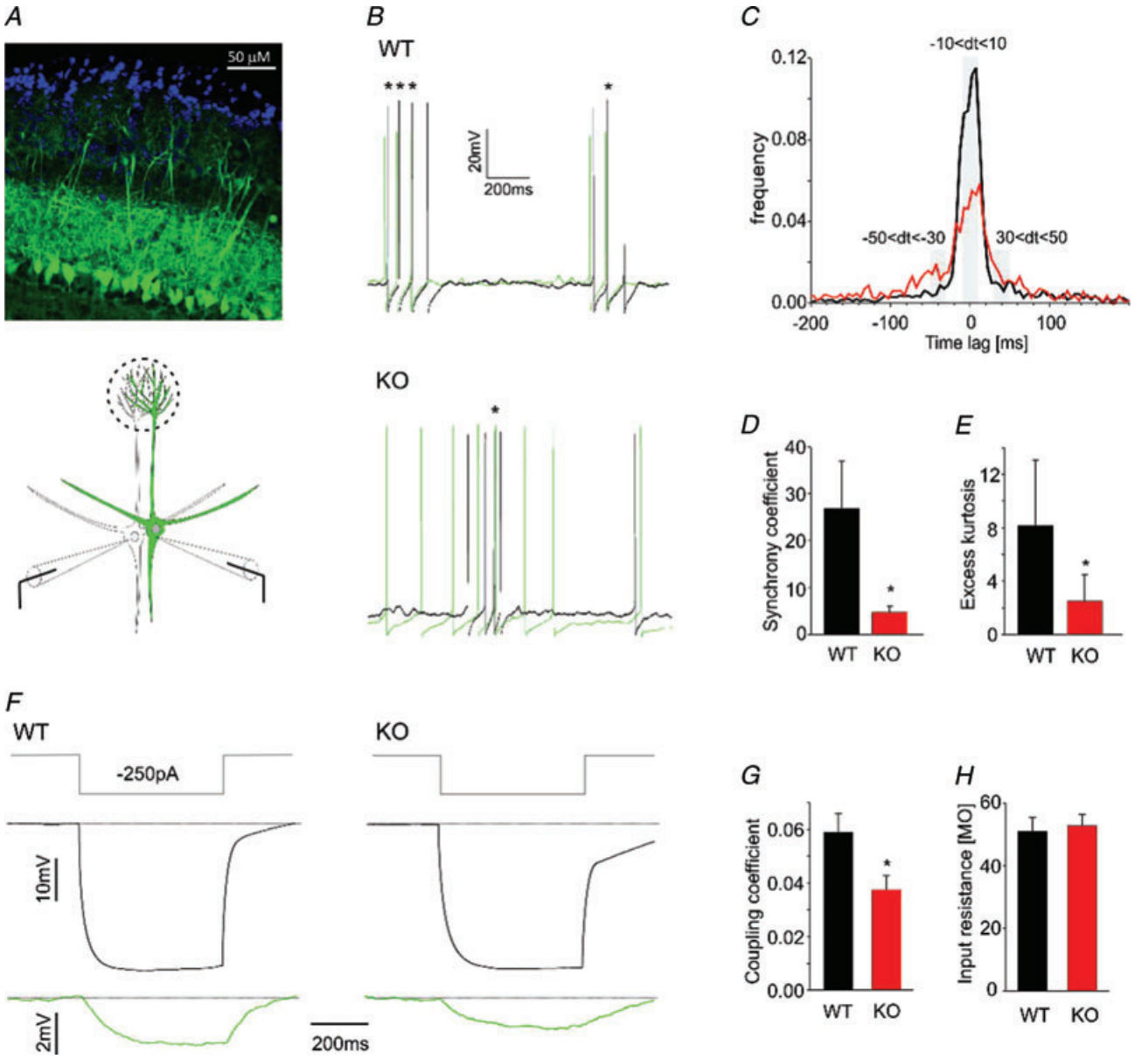

Figure 4. Fast spiking of mitral cells in OCAM knockout is desynchronized
A, confocal image of olfactory bulb horizontal slice from OCAM knockout Thy1-YFP mouse (upper panel). The primary dendrites of mitral cells, labelled with YFP (green), project to their target glomeruli that are surrounded by nuclei of juxtaglomerular cells (DAPI staining, blue). The lower panel shows a schematic drawing of the experimental approach to assess synchronous activity in pairs of mitral cells. *B*, simultaneous depolarizing current injections into pairs of mitral cells (50–100 pA, 2 s) evoked spikes in current clamp recordings of wild-type (WT, upper panel) and knockout (KO, lower panel). The panel shows superimposed epochs of action potentials in the two cells during the current pulse. In wild-type pairs, action potentials in one cell (green) were closely associated with action potentials in the other cell (black) as indicated by their close spacing. This pattern was much less obvious in the knockout. Asterisks mark lags between action potentials of <20 ms. *C*, normalized distributions of time lags between action potentials for wild-type ($n = 6$, black) and knockout ($n = 7$, red) mitral cell pairs. OCAM knockouts had a lower peak and broader distribution, indicating longer time lags between action potentials. *D*, spike synchrony was calculated as a probability of time lags less than 20 ms ($-10 < dt < 10$) divided by probability of time lags of 60–100 ms ($-50 < dt < -30$ and $30 < dt < 50$) as highlighted in grey in *C*. The synchrony coefficient was 5 times smaller in the knockout. *E*, the broader distribution in the knockout was confirmed by analysis of excess kurtosis (see methods). $^*P < 0.05$. *F* and *G*, to examine electrical coupling between mitral cells in wild-type (left panel) and knockout (right panel), current injection (−250 pA, top panel) into one cell elicited a large hyperpolarization (middle panel) and a small hyperpolarization in the other cell. This electrical coupling was reduced in the knockout (22 and 20 coupling coefficients in 11 and 10 paired recordings from wild-type and knockout respectively). *H*,

single-peaked events (paired *t* test, Fig. 5*C*, lower panel). Some mitral cells showed slow oscillations in the absence of TBOA (Supplementary Fig. 2), indicating that the oscillations are an intrinsic property of the glomerular network.

External tufted cells surrounding glomeruli show rhythmic bursting and have been suggested as drivers of oscillations in glomeruli (Hayar *et al.* 2004*a*,*b*). External tufted cells receive direct synaptic input from olfactory receptor neuron axons and can initiate oscillatory activity that is transmitted to mitral cells (De Saint Jan *et al.* 2009). We identified external tufted cells based on their morphology and the location of their cell bodies at the edge of a glomerulus (Fig. 6*A*). TBOA evoked robust oscillations in external tufted cells that also showed an excess of multi-peaked events in OCAM knockout mice (Fig. 6*B* and *C*). Similar to mitral cells, multi-peaked events were also longer in external tufted cells (Fig. 6*D*). These results indicate that loss of OCAM alters the pattern of slow oscillations in mitral as well as external tufted cells.

Synchronization of mitral cells activity as assessed with coherence analysis

Synchronization of activity in the glomerular layer occurs over a broad frequency range (Schoppa & Westbrook, 2001; Schoppa, 2006*a*,*b*; Galán *et al.* 2006; Kay *et al.* 2009). Our results demonstrate that the loss of OCAM affects correlated activity on fast and slow time scales. In order to examine correlated activity across a broad range of frequencies, we took advantage of the prominent sub-threshold depolarizations in mitral cells, as shown for a pair of cells that projected to the same glomerulus in Fig. 7*A*. At the resting membrane potential, pairs of mitral cells in wild-type mice exhibited spontaneous activity that appeared virtually identical. Spontaneous activity in the OCAM knockout also appeared similar between pairs of mitral cells, but on closer inspection it was clear that the fine structure of the activity differed (Fig. 7*A*, right traces). In contrast, spontaneous activity in mitral cells projecting to different glomeruli show little similarity (Fig. 7*B*), consistent with prior observations that correlated activity originates within the glomerulus. The synchrony in spontaneous activity between mitral cells within a glomerulus suggests tight coupling of chemical and electrical synapses. We used coherence analysis (see Methods) to assess the shared spectral content between mitral cell pairs in wild-type and knockout mice. Coherence analysis allowed us to compare the low frequency components resulting from slow oscillations as well as higher frequency components generated by fast synaptic activity.

Wild-type pairs projecting to the same glomerulus (sg) showed a much larger coherence than pairs projecting to different glomeruli (dg, Fig. 7*C*, black *vs.* blue traces), consistent with intraglomerular synchronization. Mitral cell pairs in the knockout, on the other hand, showed glomerulus-specific coherence only at 0–4 Hz (KO sg, Fig. 7*C*, red *vs.* yellow traces), reflecting the relative preservation of correlated slow oscillations as seen in the example traces in Fig. 7*A*. As expected, the coherence for cell pairs that projected to different glomeruli was the same as baseline values for wild-type or knockout (Fig. 7*C*, blue *vs.* yellow traces). The differences in coherence between wild-type and OCAM knockout were not due to differences in the spectral content because the power spectrum of the signals were nearly identical (Fig. 7*D*). We also analysed the phase of the coherence by calculating the phase uncertainty, which should be near 0 deg for time-locked activity and near 180 deg for out of phase activity. The phase uncertainty showed a similar pattern as the coherence magnitude (Supplemental Fig. 3). The coherence analysis demonstrates the high degree of synchronization of spontaneous activity within a glomerulus and the frequency-dependent reduction of synchronous activity in the absence of OCAM.

Discussion

We used several different physiological measures to examine the functional effects of OCAM knockout on mitral cell activity. The loss of OCAM reduced the synchrony of fast and slow mitral cell activity within a glomerulus without altering afferent excitatory input or dendrodendritic inhibition. The alteration of intra-glomerular activity in the OCAM knockout may provide clues to the functional significance of axodendritic and dendrodendritic compartmentalization.

Correlated activity in olfactory bulb glomeruli

Our results show that the loss of OCAM reduced the synchrony of glomerular activity. Correlated activity within a glomerulus depends on synaptic and electrical interactions between mitral cell apical dendrites (Schoppa & Westbrook, 2002; Christie *et al.* 2005), interactions

the input resistance was the same in wild-type and knockout mitral cells used for measurements of electrical coupling. Even though there was an approximately 30% reduction in coupling coefficients in OCAM knockouts, the lack of change in input resistance was not surprising because gap junctional conductance constitutes only about 20–25% of the total conductance in mitral cells at this age (Maher *et al.* 2009).

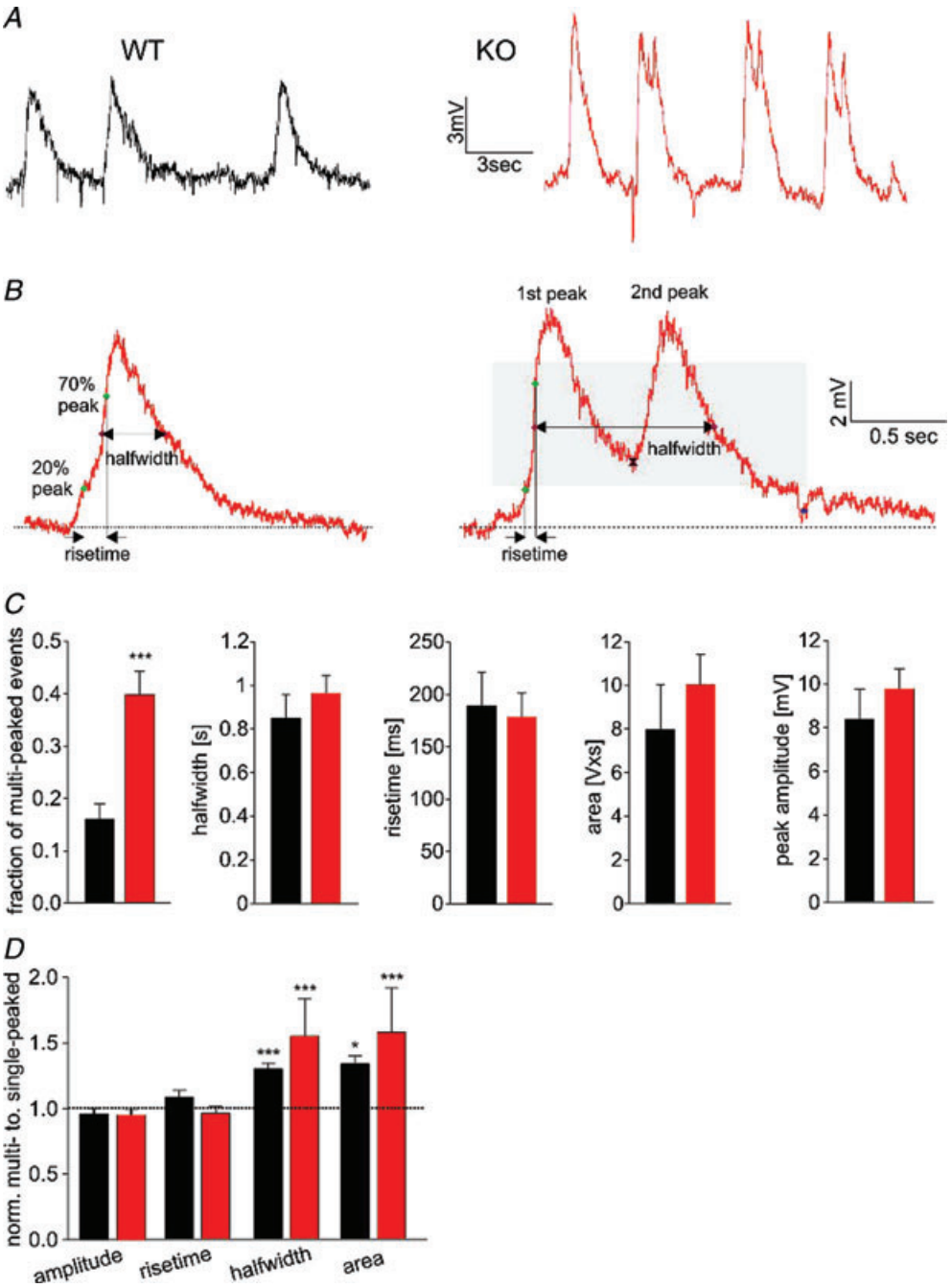

Figure 5. TBOA-induced slow oscillations in mitral cells have altered shape in OCAM knockouts
A, application of the glutamate uptake blocker TBOA evoked ongoing slow oscillations of mitral cells. These slow oscillations originate in the glomerular layer because mitral cells with severed apical dendrites show no oscillations (not shown; Schoppa & Westbrook, 2001). Note the presence of frequent multi-peaked oscillations in the knockout. *B*, we used the following parameters to analyse the shape of individual events: peak amplitude, area, rise time and half-width. For multi-peaked events, a second peak was considered present if the minimum between peaks occurred in the grey area (right panel, see Methods). *C*, bar graphs depicting mean values for slow oscillations in wild-type ($n = 13$, black) and knockout ($n = 14$, red) mitral cells. There was a 3-fold increase in multi-peaked oscillations in the knockout. Membrane potentials were -63.9 ± 1.9 mV and -63.0 ± 1.5 mV for wild-type and knockout respectively. 76 ± 9 and 70 ± 8 events per cell were analysed for wild-type and knockout, respectively. *D*, for each cell, the parameters of single- and multi-peaked oscillations were normalized to the average values for single-peaked oscillations. The area and half-width was larger for multi-peaked events in the knockout as well as for the occasional multi-peaked events in wild-type cells (paired *t* test).

with external tufted cells and interneurons (Hayar *et al.* 2005; Schoppa, 2006*b*; Galán *et al.* 2006), as well as the distribution of synapses and receptors (De Saint Jan & Westbrook, 2007). Connexin 36 knockout mice completely lack electrical coupling and fast correlated spiking, but mitral cell activity in these mice differed substantially from that of the OCAM knockout. For example, spontaneous mitral cell activity is nearly abolished in connexin 36 knockouts (Christie *et al.* 2005; Maher *et al.* 2009), but present in OCAM knockouts. Furthermore, evoked slow oscillations were correlated in the connexin 36 knockout. The coherence analysis demonstrates that the loss of OCAM affects correlated activity across a broad frequency range including both slow oscillations and the fast subthreshold activity generated by chemical and electrical synapses. The increased frequency of multi-peaked slow oscillations in the OCAM knockout indicate either a disrupted pattern of glutamate release from dendrodendritic synapses or the access of glutamate to receptors in the dendrodendritic subcompartment.

Glutamate spillover from axons of olfactory receptor neurons and mitral cell primary dendrites is thought to be involved in generation and synchronization of slow membrane voltage oscillations (Schoppa & Westbrook, 2001; Christie *et al.* 2005). Desegregation of axodendritic and dendrodendritic synapses would be expected to alter the spread of glutamate between axodendritic synapses, and may also allow glutamate that is released at axodendritic synapses to access dendrodendritic synapses. Theoretical prediction for timing of neurotransmitter diffusion is in the range of milliseconds (Kullmann *et al.* 1999; Overstreet *et al.* 2000), whereas the rise time of the slow envelope requires hundreds of milliseconds. Thus, glutamate spillover may be critical for initiation of an oscillation but asynchronous excitatory activity must contribute to its long duration. The reduced synchrony

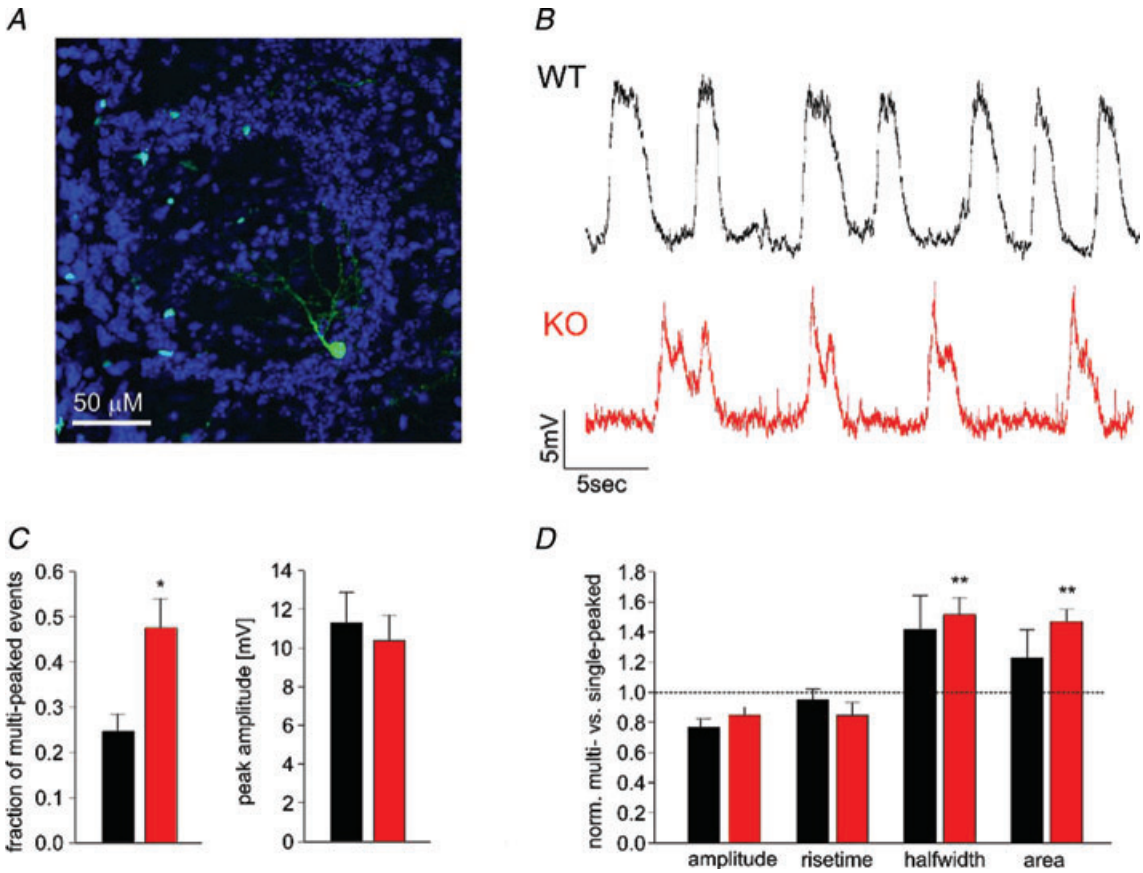

Figure 6. External tufted cells mimic the phenotype of slow oscillations in mitral cells
A, confocal image showing typical external tufted cell (green) in the OCAM knockout, with periglomerular cell body and intraglomerular processes. *B*, current clamp recordings from an external tufted cell in wild-type (black) and in the knockout (red) show slow oscillations in the presence of TBOA. *C*, the parameters of the slow oscillations were analysed as in Fig. 3. As for mitral cells, there was an increase in multi-peaked events in OCAM knockout external tufted cells ($n = 9$, red) compared to controls ($n = 8$, black). Membrane potential was on -68.5 ± 1.77 mV and -68.62 ± 1.8 mV for wild-type and knockout respectively. 54.5 ± 10.0 and 56.8 ± 5.5 events per cell were analysed for wild-type and knockout, respectively. *D*, the half-width and area were larger for multi-peaked events in external tufted cells.

in slow oscillations could originate in mitral cells or external tufted cells, which have been suggested as drivers of slow glomerular oscillations (Hayar *et al.* 2004*b*; de Saint Jan *et al.* 2009). Interglomerular circuits involving juxtaglomerular cells can also affect signalling between afferent axons and external tufted cells (Shao *et al.* 2009; Kiyokage *et al.* 2010). Enhanced glutamate spillover could increase activation of mGluR1 that is important for slow

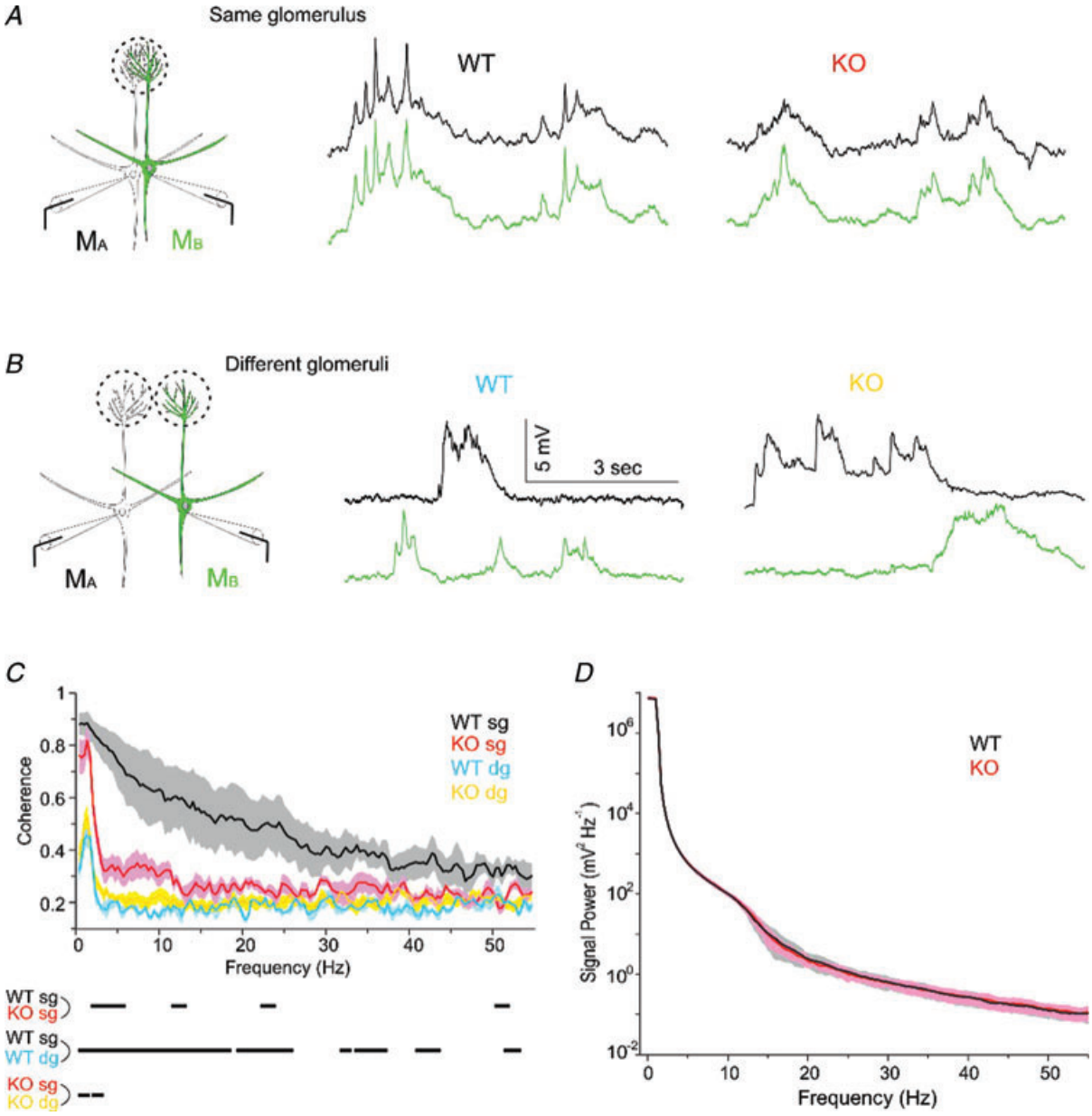

Figure 7. Coherence analysis reveals a reduction glomerulus-specific synchrony of mitral cells in OCAM knockouts

We recording spontaneous activity in current clamp recording from pairs of mitral cells *A*. In cells projecting to the same glomerulus, spontaneous activity in the two cells appeared nearly identical in the wild-type. *B*, for mitral cells that projected to different glomeruli, there was little overlap in spontaneous activity, indicating that correlated activity originated within the glomerulus. *C*, to assess the spectral content of the activity, we calculated the coherence in several conditions. The plot shows the coherence (±1 SEM, shaded area) for 4 wild-type pairs projecting to the same glomerulus (WT sg, black), 5 OCAM knockout pairs projecting to the same glomerulus (KO sg, red), 4 wild-type pairs projecting to different glomeruli (WT dg, purple), and 8 knockout pairs projecting to different glomeruli (KO dg, yellow). The dashes below the X-axis indicate frequencies at which the coherence was significantly different across conditions ($P < 0.05$). *D*, power spectra were computed for spontaneous activity of mitral cells used in the coherence analysis. There was no different in the spectral content between wild-type ($n = 12$) and OCAM knockout cells ($n = 14$). The plot shows the power spectrum ± 1 SEM.

oscillations (Schoppa & Westbrook, 2001; Yuan & Knopfel, 2006; Bovolin *et al.* 2009; Dong *et al.* 2009).

OCAM and the compartmentalization of glomeruli

Little is known about the functional significance of subcompartments within glomeruli. Axodendritic synapses of incoming afferents are segregated from dendrodendritic synapses between mitral/tufted cells and periglomerular cells (Kasowski *et al.* 1999). Axodendritic synapses are located on the distal ends of the tapering apical dendrites of mitral cells in the glomerulus whereas dendrodendritic synapses are more proximal. Loss of OCAM leads to a breakdown of subcompartments and affects olfactory behaviour (Walz *et al.* 2006), but the underlying molecular mechanism is unclear. Like NCAM, OCAM is a member of the Ig family of homophilic adhesion molecules. OCAM is expressed in three zones of the olfactory epithelium that project their axons to ventrolateral olfactory bulb (Fujita *et al.* 1985; Yoshihara *et al.* 1997). In the dorsomedial olfactory bulb, OCAM is transiently expressed in mitral/tufted cells until shortly after birth (Treloar *et al.* 2003). OCAM was initially suggested as important for axon bundling and pathfinding (Yoshihara & Mori, 1997), yet genetic deletion of OCAM did not affect targeting of olfactory nerve axons (Walz *et al.* 2006). However, clustering of axonal and dendritic profiles in glomeruli is reduced in all regions of the bulb, suggesting that OCAM-mediated dendrite–dendrite adhesion in the dorsomedial bulb acts in a reciprocal fashion. Consistent with this idea, our experiments in the OCAM knockout showed similar results in dorsomedial and ventrolateral glomeruli. Although other adhesion molecules have been implicated in olfactory development, knockouts of NCAM or Semaphorin 3A do not show the intraglomerular pattern seen in the OCAM knockout (Gheusi *et al.* 2000; Schwarting *et al.* 2004). Interestingly, OCAM also appears to control compartmentalization of afferents and dendrites in the retrosplenial cortex (Ichinohe *et al.* 2008).

We did not find evidence for alteration of incoming afferent synapses or dendrodendritic inhibition. Our functional results are consistent with a lack of change in the number of synapses identified by electron microscopy in the OCAM knockout (Walz *et al.* 2006). Our data cannot resolve whether the redistribution of otherwise normal axodendritic and dendrodendritic synapses is solely responsible for the reduced synchrony of glomerular activity. Disruption of cell–cell adhesion during glomerular formation could also initiate secondary changes in the expression or distribution of synaptic molecules including receptors and channels that may contribute to the functional phenotype. Such questions could be addressed with new techniques for the 3-D reconstruction of microcircuits such as olfactory bulb glomeruli (Briggman & Denk, 2006).

Olfactory processing in the OCAM knockout

The glomerular circuitry is likely to contribute to both odour detection and discrimination. Glomerular processing for odour recognition must be quite fast as mice require as little as one sniff, taking under 200 ms to discriminate simple odours (Abraham *et al.* 2004; Rinberg *et al.* 2006). Interestingly, OCAM knockout mice show enhanced olfactory acuity as assessed by decreased latency in finding a buried cookie on first exposure (Walz *et al.* 2006). The reduced intraglomerular synchrony we observed might seem to predict a reduction in odorant sensitivity. However, the increased duration of slow oscillations in the OCAM knockout animals might explain this apparent discrepancy. Sniffing occurs in the same time frame as slow membrane voltage oscillations in mitral cells. Thus, if afferent activity associated with a sniff causes a sufficient depolarization of mitral cells (Charpak *et al.* 2001; Cang & Isaacson, 2003), the likelihood of mitral cell firing would be higher in the OCAM knockout. One might also predict that odour sensitivity would be reduced at low odour concentrations because of the lack of fast synchronization of mitral cells.

References

Abraham NM, Spors H, Carleton A, Margrie TW, Kuner T & Schaefer AT (2004). Maintaining accuracy at the expense of speed: stimulus similarity defines odor discrimination time in mice. *Neuron* **44**, 865–876.

Baker H, Grillo M & Margolis FL (1989). Biochemical and immunocytochemical characterization of olfactory marker protein in the rodent central nervous system. *J Comp Neurol* **285**, 246–261.

Bovolin P, Bovetti S, Fasolo A, Katarova Z, Szabo G, Shipley MT, Margolis FL & Puche AC (2009). Developmental regulation of metabotropic glutamate receptor 1 splice variants in olfactory bulb mitral cells. *J Neurosci Res* **87**, 369–379.

Briggman KL & Denk W (2006). Towards neural circuit reconstruction with volume electron microscopy techniques. *Curr Opin Neurobiol* **16**, 562–570.

Buck L & Axel R (1991). A novel multigene family may encode odorant receptors: a molecular basis for odor recognition. *Cell* **65**, 175–187.

Cang J & Isaacson JS (2003). In vivo whole-cell recording of odor-evoked synaptic transmission in the rat olfactory bulb. *J Neurosci* **23**, 4108–4116.

Carlson GC, Shipley MT & Keller A (2000). Long-lasting depolarizations in mitral cells of the rat olfactory bulb. *J Neurosci* **20**, 2011–2021.

Chao TI, Kasa P & Wolff JR (1997). Distribution of astroglia in glomeruli of the rat main olfactory bulb: exclusion from the sensory subcompartment of neuropil. *J Comp Neurol* **388**, 191–210.

Charpak S, Mertz J, Beaurepaire E, Moreaux L & Delaney K (2001). Odor-evoked calcium signals in dendrites of rat mitral cells. *Proc Natl Acad Sci U S A* **98**, 1230–1234.

Chen WR & Shepherd GM (2005). The olfactory glomerulus: a cortical module with specific functions. *J Neurocytol* **34**, 353–360.

Christie JM, Bark C, Hormuzdi SG, Helbig I, Monyer H & Westbrook GL (2005). Connexin36 mediates spike synchrony in olfactory bulb glomeruli. *Neuron* **46**, 761–772.

Christie JM & Westbrook GL (2006). Lateral excitation within the olfactory bulb. *J Neurosci* **26**, 2269–2277.

De Saint Jan D & Westbrook GL (2005). Detecting activity in olfactory bulb glomeruli with astrocyte recording. *J Neurosci* **25**, 2917–2924.

De Saint Jan D & Westbrook GL (2007). Disynaptic amplification of metabotropic glutamate receptor 1 responses in the olfactory bulb. *J Neurosci* **27**, 132–140.

De Saint Jan D, Hirnet D, Westbrook GL & Charpak S (2009). External tufted cells drive the output of olfactory bulb glomeruli. *J Neurosci* **29**, 2043–2052.

Dong HW, Hayar A, Callaway J, Yang XH, Nai Q & Ennis M (2009). Group I mGluR activation enhances Ca^{2+}-dependent nonselective cation currents and rhythmic bursting in main olfactory bulb external tufted cells. *J Neurosci* **29**, 11943–11953.

Fantana AL, Soucy ER & Meister M (2008). Rat olfactory bulb mitral cells receive sparse glomerular inputs. *Neuron* **59**, 802–814.

Feng G, Mellor RH, Bernstein M, Keller-Peck C, Nguyen QT, Wallace M, Nerbonne JM, Lichtman JW & Sanes JR (2000). Imaging neuronal subsets in transgenic mice expressing multiple spectral variants of GFP. *Neuron* **28**, 41–51.

Fujita SC, Mori K, Imamura K & Obata K (1985). Subclasses of olfactory receptor cells and their segregated central projections demonstrated by a monoclonal antibody. *Brain Res* **326**, 192–196.

Galán RF, Fourcaud-Trocme N, Ermentrout GB & Urban NN (2006). Correlation-induced synchronization of oscillations in olfactory bulb neurons. *J Neurosci* **26**, 3646–3655.

Gheusi G, Cremer H, McLean H, Chazal G, Vincent JD & Lledo PM (2000). Importance of newly generated neurons in the adult olfactory bulb for odor discrimination. *Proc Natl Acad Sci U S A* **97**, 1823–1828.

Green EL (1966). *Biology of the Laboratory Mouse, by the Staff of the Jackson Laboratory*, 2nd edn. Dover Publications, New York.

Hayar A, Karnup S, Shipley MT & Ennis M (2004*a*). Olfactory bulb glomeruli: external tufted cells intrinsically burst at theta frequency and are entrained by patterned olfactory input. *J Neurosci* **24**, 1190–1199.

Hayar A, Karnup S, Ennis M & Shipley MT (2004*b*). External tufted cells: a major excitatory element that coordinates glomerular activity. *J Neurosci* **24**, 6676–6685.

Hayar A, Shipley MT & Ennis M (2005). Olfactory bulb external tufted cells are synchronized by multiple intraglomerular mechanisms. *J Neurosci* **25**, 8197–8208.

Huybers P (2004). Comments on 'Coupling of the hemispheres in observations and simulations of glacial climate change' by A. Schmittner, O. A. Saenko, and A. J. Weaver. *Quat Sci Rev* **23**, 207–212.

Ichinohe N, Knight A, Ogawa M, Ohshima T, Mikoshiba K, Yoshihara Y, Terashima T & Rockland KS (2008). Unusual patch-matrix organization in the retrosplenial cortex of the reeler mouse and Shaking rat Kawasaki. *Cereb Cortex* **18**, 1125–1138.

Isaacson JS (1999). Glutamate spillover mediates excitatory transmission in the rat olfactory bulb. *Neuron* **23**, 377–384.

Kasowski HJ, Kim H & Greer CA (1999). Compartmental organization of the olfactory bulb glomerulus. *J Comp Neurol* **407**, 261–274.

Kay LM, Beshel J, Brea J, Martin C, Rojas-Libano D & Kopell N (2009). Olfactory oscillations: the what, how and what for. *Trends Neurosci* **32**, 207–214.

Kim H & Greer CA (2000). The emergence of compartmental organization in olfactory bulb glomeruli during postnatal development. *J Comp Neurol* **422**, 297–311.

Kiyokage E, Pan YZ, Shao Z, Kobayashi K, Szabo G, Yanagawa Y, Obata K, Okano H, Toida K, Puche AC & Shipley MT (2010). Molecular identity of periglomerular and short axon cells. *J Neurosci* **30**, 1185–1196.

Kosaka K, Toida K, Aika Y & Kosaka T (1998). How simple is the organization of the olfactory glomerulus?: the heterogeneity of so-called periglomerular cells. *Neurosci Res* **30**, 101–110.

Kullmann DM, Min MY, Asztely F & Rusakov DA (1999). Extracellular glutamate diffusion determines the occupancy of glutamate receptors at CA1 synapses in the hippocampus. *Philos Trans R Soc Lond B Biol Sci* **354**, 395–402.

Laurent G (2002). Olfactory network dynamics and the coding of multidimensional signals. *Nat Rev Neurosci* **3**, 884–895.

Maher BJ, McGinley MJ & Westbrook GL (2009). Experience-dependent maturation of the glomerular microcircuit. *Proc Natl Acad Sci U S A* **106**, 16865–16870.

Mombaerts P, Wang F, Dulac C, Chao SK, Nemes A, Mendelsohn M, Edmondson J & Axel R (1996). Visualizing an olfactory sensory map. *Cell* **87**, 675–686.

Overstreet LO, Westbrook GL & Jones MV (2000). Measuring and modeling thespatiotemporal profile of GABA at the synapse. In *Transmembrane Transporters*, ed. Quick MV, pp. 259–275. Wiley-Liss.

Percival DP & Walden AT (1993). *Spectral Analysis for Physical Applications: Multitaper and Conventional Univariate Techniques*. Cambridge University Press, UK.

Price JL & Powell TP (1970). The mitral and short axon cells of the olfactory bulb. *J Cell Sci* **7**, 631–651.

Puopolo M & Belluzzi O (2001). NMDA-dependent, network-driven oscillatory activity induced by bicuculline or removal of Mg^{2+} in rat olfactory bulb neurons. *Eur J Neurosci* **13**, 92–102.

Rinberg D, Koulakov A & Gelperin A (2006). Speed-accuracy tradeoff in olfaction. *Neuron* **51**, 351–358.

Schoppa NE & Urban NN (2003). Dendritic processing within olfactory bulb circuits. *Trends Neurosci* **26**, 501–506.

Schoppa NE & Westbrook GL (2001). Glomerulus-specific synchronization of mitral cells in the olfactory bulb. *Neuron* **31**, 639–651.

Schoppa NE & Westbrook GL (2002). AMPA autoreceptors drive correlated spiking in olfactory bulb glomeruli. *Nat Neurosci* **5**, 1194–1202.

Schoppa NE (2006*a*). Synchronization of olfactory bulb mitral cells by precisely timed inhibitory inputs. *Neuron* **49**, 271–283.

Schoppa NE (2006*b*). AMPA/kainate receptors drive rapid output and precise synchrony in olfactory bulb granule cells. *J Neurosci* **26**, 12996–13006.

Schwarting GA, Raitcheva D, Crandall JE, Burkhardt C & Puschel AW (2004). Semaphorin 3A-mediated axon guidance regulates convergence and targeting of P2 odorant receptor axons. *Eur J Neurosci* **19**, 1800–1810.

Shao Z, Puche AC, Kiyokage E, Szabo G & Shipley MT (2009). Two GABAergic intraglomerular circuits differentially regulate tonic and phasic presynaptic inhibition of olfactory nerve terminals. *J Neurophysiol* **101**, 1988–2001.

Treloar HB, Gabeau D, Yoshihara Y, Mori K & Greer CA (2003). Inverse expression of olfactory cell adhesion molecule in a subset of olfactory axons and a subset of mitral/tufted cells in the developing rat main olfactory bulb. *J Comp Neurol* **458**, 389–403.

Walz A, Mombaerts P, Greer CA & Treloar HB (2006). Disrupted compartmental organization of axons and dendrites within olfactory glomeruli of mice deficient in the olfactory cell adhesion molecule, OCAM. *Mol Cell Neurosci* **32**, 1–14.

Yoshihara Y, Kawasaki M, Tamada A, Fujita H, Hayashi H, Kagamiyama H & Mori K (1997). OCAM: A new member of the neural cell adhesion molecule family related to zone-to-zone projection of olfactory and vomeronasal axons. *J Neurosci* **17**, 5830–5842.

Yoshihara Y & Mori K (1997). Basic principles and molecular mechanisms of olfactory axon pathfinding. *Cell Tissue Res* **290**, 457–463.

Yuan Q & Knopfel T (2006). Olfactory nerve stimulation-evoked mGluR1 slow potentials, oscillations, and calcium signaling in mouse olfactory bulb mitral cells. *J Neurophysiol* **95**, 3097–3104.

Zoubir AM (2009). Bootstrapping spectra: Methods, comparisons and application to knock data. *Signal Processing* **90**, 1424–1435.

Author contributions

M.B. and G.L.W. conceived and designed the experiments; M.B. and A.B. carried out the experiments; M.B. and M.J.M. performed data analysis; M.B. and G.L.W. drafted the paper. All authors approved the final version of the manuscript.

Acknowledgements

We thank Peter Mombaerts (Max Planck Institute of Biophysics, Frankfurt, Germany) for OCAM knockout mice and Guoping Feng (Duke University, Durham, NC) for Thy-1-YFP mice. We thank members of the Westbrook laboratory, Brady Maher, Jason Christie, Didier de Saint Jan and Marion Najac for their helpful discussions. This work was supported by National Institutes of Health grant NS02694 (G.L.W.) and a research award from the Max Planck Society.